Measurement 263 (2026) 120101

Contents lists available at ScienceDirect

Measurement

journal homepage: www.elsevier.com/locate/measurement

Structural health monitoring of piezoelectric structures by estimating energy conversion efficiency with capacitance measurements

M. Berardengo [a], M. Mercato [a], S. Manzoni [b,*]

[a] Universitá degli Studi di Genova - Department of Mechanical, Energy, Management and Transportation Engineering, Via all'Opera Pia, 15A - 16145 Genoa, Italy
[b] Politecnico di Milano - Department of Mechanical Engineering, Via La Masa, 1 - 20156 Milan, Italy

ARTICLE INFO

Keywords:
Piezoelectric elements
Piezoelectric structure
Electro-mechanical coupling factor
Structural health monitoring
Capacitance measurement
Energy conversion efficiency

ABSTRACT

In structures equipped with piezoelectric materials, the quantification of the efficiency of the energy conversion between mechanical and electrical domain (and vice versa) was already demonstrated to be a reliable feature for determining the presence of a structural damage. Usually, this efficiency is determined by means of vibration measurements to derive the value of the modal electro-mechanical coupling coefficient, which is the damage feature employed to calculate damage indexes. Nevertheless, in some cases, the estimation of this damage feature can be challenging because of different reasons, such as, e.g., non sufficient external excitation to the system, low values of the modal electro-mechanical coupling coefficient which makes its estimation uncertain and implies the need of shunting the piezoelectric elements with tailored electrical impedances.

The present paper aims at showing that similar damage indexes can be estimated also by measuring capacitance trend as function of frequency for each piezoelectric element in the structure. This allows monitoring the structure without any need of vibration measurements and addition of external electric circuits used to shunt the piezoelectric elements, with significant simplification of the estimation procedure.

Three different damage indexes are proposed, evidencing which of them are the most reliable for detecting the presence of the damage and getting information about its location. The method and the indexes are studied through numerical analyses and validated by means of an experimental campaign on a tailored set-up.

1. Introduction

Piezoelectric materials are becoming more and more spread in structures and systems for very different purposes, such as, e.g., vibration control (e.g., [1–5]), energy harvesting (e.g., [6–9]) and micro positioning (e.g., [10,11]), as demonstrated by the increasing number of applications in practical engineering cases [12–15]. This is due to their advantages (e.g., lightweight) but also to the simplification in their integration process in structures (e.g., [16]), also thanks to the advances in additive manufacturing techniques.

Piezoelectric elements (either stacks or patches) are also widely used for structural health monitoring (SHM) through different approaches. The first and most widespread one is the use of piezoelectric elements to build sensors used for measuring structural vibrations [17]. Then, other techniques more centred on the piezoelectric transducers are presented in the literature: e.g., piezoelectric elements are used to enhance the sensitivity to the damage by adding negative resistance elements in piezoelectric circuitry network to amplify the damage signature in a periodic structure in presence of large mechanical damping [18], are employed to generate/measure ultrasonic guided waves [19,20] (e.g., for estimating bolt pretension [21]), and are at the foundation of the electro-mechanical impedance (EMI) technique [22–26]. In EMI approaches, the structural alterations are found by measuring the current flowing through a piezoelectric element attached to the structure while applying voltage to it, or vice versa.

Recently, a new approach for using piezoelectric elements for SHM purposes was presented in [27] and is based on the estimation of the efficiency of the energy conversion between mechanical and electrical domains which are linked by the capability of each piezoelectric element to convert mechanical energy into electrical and vice versa, thanks to direct and inverse effects. In [27], a new damage feature was indeed proposed, which is the modal electro-mechanical coupling coefficient (MEMCF) k_i. Considering a system (mechanical, aeronautical, civil, etc.) with a piezoelectric element attached, k_i expresses the efficiency of the energy conversion between the piezoelectric element and the ith mode of the vibrating structure and vice versa. In case multiple piezoelectric elements are attached to the structure, a MEMCF $k_{i,p}$ for each mode and each piezoelectric element can be defined, where the subscript p indicates the pth piezoelectric element. The absolute

* Corresponding author.
E-mail address: stefano.manzoni@polimi.it (S. Manzoni).

https://doi.org/10.1016/j.measurement.2025.120101
Received 14 October 2025; Received in revised form 10 December 2025; Accepted 13 December 2025
Available online 17 December 2025

value of each MEMCF can be estimated as

$$|k_{i,p}| = \sqrt{\frac{\hat{\omega}_{i,p}^2 - \omega_{i,\text{all}}^2}{\omega_{i,\text{all}}^2}} \tag{1}$$

where $\omega_{i,\text{all}}$ is the ith eigenfrequency of the system with all the piezoelectric elements short-circuited and $\hat{\omega}_{i,p}$ is the ith eigenfrequency of the system with all the piezoelectric elements short-circuited exception made for the pth which is open-circuited.

The MEMCF is a quantity depending on many features of the system (e.g., mechanical and electrical properties, geometry). Among them, the MEMCF shows a significant dependence on the mode shape components at the boundaries of the piezoelectric element [28]. As an example, according to [28], the MEMCF of a piezoelectric patch at the ith mode for a mono-dimensional structure (e.g., beam) depends on the quantity ψ_i, defined as:

$$\psi_i = \phi_i'(x_2) - \phi_i'(x_1) \tag{2}$$

where ϕ_i is the ith eigenvector of the system, scaled to the unit modal mass, with the piezoelectric transducer short-circuited, ϕ_i' is the first derivative of ϕ_i with respect to the coordinate x along the beam length, and x_1 and x_2 are the coordinate values of the boundaries of the piezoelectric patch. Thus, ψ_i physically represents the difference of the mode shape slopes at the boundaries of the piezoelectric element. For bi-dimensional structures (e.g., plate), the expression of ψ_i is more complicated [29] but its meaning is still related to the mode shape slope at the boundaries of the piezoelectric element.

This implies that, when a damage occurs in the structure, k_i changes for all the modes, especially for those for which the corresponding modes have changed at the boundaries of the considered piezoelectric element. Therefore, some $k_{i,p}$ values significantly change because of the appearance of a damage, while others remain close to their original values related to the healthy (or reference) condition. This implies that sensitivity to damage is close to that of methods based on mode shape estimation (or related quantities) (e.g., see [30]). The authors focused on this damage feature for many reasons (e.g., clear physical meaning) but, overall, for its scarce sensitivity to variability of environmental and operating conditions.

In [27], the authors show that the following index based on MEMCF can be used for damage detection:

$$s_p = \sum_{i=h}^{g} \left| \left(|k_{i,p}| - |k_{i,p,\text{u}}| \right) \right| \tag{3}$$

where $k_{i,p,\text{u}}$ is the value of $k_{i,p}$ in the undamaged/reference condition. Moreover, h and g indicate two generic modes (with $h < g$). It is noticed that, in Eq. (3), it is also possible to consider non-subsequent modes.

Index s_p is sensitive to the presence of damages and this was demonstrated with tests on a simple structure (i.e., a beam) and on more complex structures (i.e., a truss). The time trend of s_p can be analysed to detect the presence of damages using, e.g., Mahalanobis distance [31,32] (but other approaches are possible as well). When more than one piezoelectric element is attached to the structure, the index shows to be sensitive also to damage location because the largest s_p value is obtained for the piezoelectric elements closest to the damage. Furthermore, $k_{i,p}$ and, thus, s_p were shown to be lowly affected by environmental effects (mainly thermal effects) and changes of operational conditions and this makes them reliable for damage detection because their use allows avoiding the masking effect due to environmental/operating variations without the need of any processing, which is a relevant and widely treated point in the literature related to SHM [33–36]. The reader is invited to consult [27] for an analytical analysis of the robustness of the MEMCF to temperature variations. The same paper also evidences that s_p and $k_{i,p}$ values can be even used as inputs to more complicated SHM algorithms (e.g., based on artificial intelligence [37]) to improve damage detection reducing masking effects of temperature.

According to Eq. (1), to estimate $|k_{i,p}|$ and calculate s_p, modal analyses of the structure must be carried out to determine the different eigenfrequency values $\hat{\omega}_{i,p}$ and $\omega_{i,\text{all}}$. This is a simple procedure which can be even performed exploiting environmental excitation and operational modal analysis approaches. Nevertheless, this procedure can be challenging when small initial values of $|k_{i,p}|$ characterise the structure. This could occur when, as an example, the piezoelectric elements used are not able to exert enough action to the structure (i.e., non-optimised piezoelectric elements placed in given positions of the structure for other purposes). Even if this problem can be overcome by shunting the piezoelectric elements to negative capacitances [27] since they are able to artificially increase the MEMCFs, this requires the addition of as many electrical circuits as the number of piezoelectric elements present on the structure. Indeed, negative capacitances do not exist in nature and they are simulated through electric circuits [38]. This also implies the need of a remote system capable of connecting and disconnecting each piezoelectric element to and from the associated negative capacitance, depending on the test. Furthermore, at least one sensor (e.g., an accelerometer) measuring structural vibrations is needed for estimating the eigenfrequencies. Moreover, external excitation, either generated on purpose or obtained by environmental sources, is needed to perform the modal analyses and, sometimes, this can be difficult because of a number of reasons, such as, e.g., complication of the experimental set-up and non sufficient environmental forcing. Finally, last but not least, estimating $|k_{i,p}|$ with Eq. (1) implies to carry out two different modal analyses for each piezoelectric element. In case the tests are not quick, environmental changes occurring during the two tests related to one piezoelectric element can produce bias on the estimated $|k_{i,p}|$ values because $\omega_{i,\text{all}}$ and $\hat{\omega}_{i,p}$ are estimated at different temperature values.

To avoid the above issues and the addition of negative capacitances, this paper proposes a different strategy to estimate $|k_{i,p}|$ and calculate s_p (or related quantities), based on the measurement of the capacitance trend as function of frequency of each piezoelectric element in the structure. It will be shown that the devices to be used for such estimations are similar to those commonly employed in EMI approaches, but with less requirements in terms of performance. Starting from the measured capacitance curve in frequency, three different approaches are proposed here to find either the MEMCF of different modes or quantities directly related to these MEMCFs, implying the possibility of calculating some damage indexes. The three approaches differ for complexity of the procedure to derive MEMCFs (or related quantities). Their reliability in indicating damage presence and location are tested and compared. The approaches found as reliable are characterised by a fast and easy test procedure, thus resulting advantageous compared to the employment of vibration measurements.

The paper is structured as follows: Section 2 presents the model at the base of the proposed method, and Section 3 proposes and compares three alternative ways to determine $|k_{i,p}|$ and calculate s_p (or related quantities). Finally, Sections 4 and 5 discuss numerical simulations and experimental tests, respectively, to give evidence of the reliability of the newly proposed SHM approach.

2. Model of the system

According to [39], the electric admittance Y_p (where $Y_p = 1/Z_p$, being Z_p the impedance) of a piezoelectric element attached to a vibrating structure (all the other piezoelectric elements attached to the structure are considered as short-circuited) can be described as follows in the frequency domain:

$$Y_p(\mathrm{j}\Omega) = \frac{I_p(\mathrm{j}\Omega)}{V_p(\mathrm{j}\Omega)} = \frac{\mathrm{j}\Omega Q_p(\mathrm{j}\Omega)}{V_p(\mathrm{j}\Omega)} = \mathrm{j}\Omega\left(C_{\infty,p} + \frac{1}{\mathrm{j}\omega R_p} + \sum_{i=1}^{N} \frac{\chi_{i,p}^2}{-\Omega^2 + 2\mathrm{j}\zeta_i\omega_{i,\text{all}}\Omega + \omega_{i,\text{all}}^2}\right) \tag{4}$$

where Ω is the angular frequency, j is the imaginary unit, V_p is the voltage between the electrodes of the considered piezoelectric element,

Q_p is the charge in one of the electrodes ($-Q_p$ in the other), I_p is the current flowing through the piezoelectric element, $C_{\infty,p}$ is the capacitance at constant strain (also seen as the capacitance at infinite frequency) of the considered piezoelectric element, R_p is the associated inherent resistance, ζ_i is the non-dimensional damping ratio associated to the eigenfrequency $\omega_{i,\mathrm{all}}$, N is the number of modes, and, finally, $\chi_{i,p}$ is a modal coupling coefficient. It is possible to look at $k_{i,p}$ as a normalised and dimensionless version of $\chi_{i,p}$ [40].

Considering a single-degree-of-freedom reduction to describe the frequency trend of Y_p for $\Omega \simeq \omega_{i,\mathrm{all}}$, the modal sum in Eq. (4) can be substituted by the sum of three terms: one describing the contribution of the ith mode, and the others the residual contributions of the out-of-band modes. Thus, for $\Omega \simeq \omega_{i,\mathrm{all}}$, Y_p can be expressed as:

$$\begin{aligned} Y_p(\mathrm{j}\Omega)\big|_{\Omega\simeq\omega_{i,\mathrm{all}}} &= \mathrm{j}\Omega(C_{\infty,p} + \frac{1}{\mathrm{j}\omega R_p} + \frac{1}{-\Omega^2 \hat{L}_{i,p}} \\ &\quad + \frac{\chi_{i,p}^2}{-\Omega^2 + 2\mathrm{j}\zeta_i\omega_{i,\mathrm{all}}\Omega + \omega_{i,\mathrm{all}}^2} + \hat{C}_{i,p}) \\ &= \mathrm{j}\Omega(C_{i,p} + \frac{1}{\mathrm{j}\omega R_p} + \frac{1}{-\Omega^2 \hat{L}_{i,p}} \\ &\quad + \frac{\chi_{i,p}^2}{-\Omega^2 + 2\mathrm{j}\zeta_i\omega_{i,\mathrm{all}}\Omega + \omega_{i,\mathrm{all}}^2}) \end{aligned} \tag{5}$$

where $\hat{L}_{i,p}$ and $\hat{C}_{i,p}$ are constants accounting for the contribution of the modes lower and higher than the ith, respectively:

$$\sum_{n=1}^{i-1} \frac{\chi_{n,p}^2}{-\Omega^2 + 2\mathrm{j}\zeta_n\omega_{n,\mathrm{all}}\Omega + \omega_{n,\mathrm{all}}^2} \simeq \sum_{n=1}^{i-1} \frac{\chi_{n,p}^2}{-\Omega^2} = \frac{1}{-\Omega^2 \hat{L}_{i,p}} \tag{6}$$

$$\sum_{n=i+1}^{N} \frac{\chi_{n,p}^2}{-\Omega^2 + 2\mathrm{j}\zeta_n\omega_{n,\mathrm{all}}\Omega + \omega_{n,\mathrm{all}}^2} \simeq \sum_{n=i+1}^{N} \frac{\chi_{n,p}^2}{\omega_{n,\mathrm{all}}^2} = \hat{C}_{i,p} \tag{7}$$

Furthermore,

$$C_{i,p} = C_{\infty,p} + \hat{C}_{i,p} \tag{8}$$

The symbol $C_{i,p}$ indicates the modal capacitance of the pth piezoelectric element at the ith mode. From Eq. (5), it is possible to derive the frequency trend of the capacitance C_p of the pth piezoelectric element for $\Omega \simeq \omega_{i,\mathrm{all}}$ as:

$$\begin{aligned} C_p(\mathrm{j}\Omega)\big|_{\Omega\simeq\omega_{i,\mathrm{all}}} &= \frac{\mathrm{Im}\{Y_p(\mathrm{j}\Omega)\}}{\Omega}\Big|_{\Omega\simeq\omega_{i,\mathrm{all}}} \\ &= C_{i,p} - \frac{1}{\Omega^2 \hat{L}_{i,p}} + \mathrm{Re}\{\frac{\chi_{i,p}^2}{-\Omega^2 + 2\mathrm{j}\zeta_i\omega_{i,\mathrm{all}}\Omega + \omega_{i,\mathrm{all}}^2}\} \end{aligned} \tag{9}$$

where $\mathrm{Im}\{\cdot\}$ and $\mathrm{Re}\{\cdot\}$ indicate the imaginary and real parts, respectively, of a complex quantity. According to [41,42]:

$$k_{i,p}^2 = \frac{\chi_{i,p}^2}{\omega_{i,\mathrm{all}}^2 C_{i,p}} \tag{10}$$

Therefore, Eq. (9) can be rearranged using Eq. (10) as:

$$C_p(\mathrm{j}\Omega)\big|_{\Omega\simeq\omega_{i,\mathrm{all}}} = C_{i,p} - \frac{1}{\Omega^2 \hat{L}_{i,p}} + \mathrm{Re}\{\frac{k_{i,p}^2\omega_{i,\mathrm{all}}^2 C_{i,p}}{-\Omega^2 + 2\mathrm{j}\zeta_i\omega_{i,\mathrm{all}}\Omega + \omega_{i,\mathrm{all}}^2}\} \tag{11}$$

It is also important to notice that, according to Eqs. (7), (8) and (10), the following relation holds between the modal capacitances of two generic subsequent modes:

$$C_{i-1,p} = C_{i,p}(1 + k_{i,p}^2) \tag{12}$$

3. Estimation of MEMCF and damage index

This section introduces a different approach for estimating $|k_{i,p}|$ and s_p (or related quantities) compared to the use of vibration tests explained in Section 1 (and in [27]). The estimation procedure presented here allows avoiding the use of additional devices (i.e., accelerometers, negative capacitances) and the need for carrying out modal analysis. This last point implies a reduction of time needed for estimating $|k_{i,p}|$ and s_p because two tests for each piezoelectric element were necessary with the procedure described in Section 1 (i.e., one with the element short-circuited, and the other with the element open-circuited), while the procedure presented here is based on a single test per piezoelectric element.

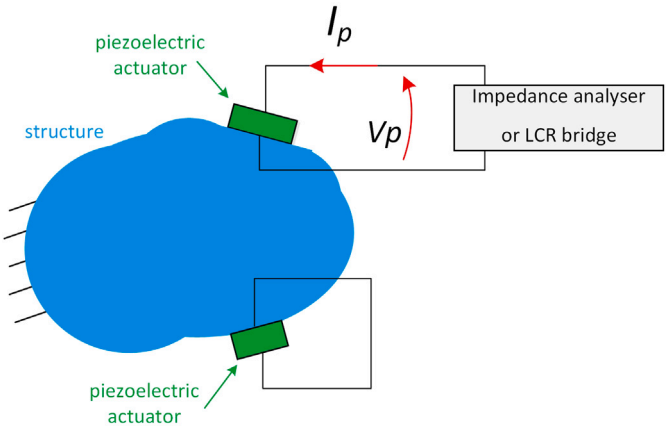

Fig. 1. Measurement procedure: when the admittance of one piezoelectric element is tested, the other piezoelectric elements are short-circuited.

The procedure proposed here is to measure the electric admittance (or impedance) of each piezoelectric element as function of frequency by generating voltage at the electrodes and measuring the current flowing through the piezoelectric element, or vice versa. This can be easily carried out using, e.g., an impedance analyser or an LCR bridge. When one piezoelectric element is tested, all the others are short-circuited. The schematic in Fig. 1 further explains how to carry out the mentioned measurement. This implies that the hardware and the measurement procedure are similar to those employed in the context of EMI approaches, in the sense that one has to generate voltage and measure current, or vice versa, in both the cases. Nevertheless, it is important to stress that the resulting measured admittance curve is used differently compared in EMI.

This section is organised in five subsections. The first three discuss three different approaches for deriving $|k_{i,p}|$ and s_p (or related quantities) from the measured admittance (or impedance) curves, while the fourth compares them and the fifth evidences differences of the present methods with respect to EMI.

3.1. First method

From the measured curve of $Y_p(\mathrm{j}\Omega)$, the corresponding curve of $C_p(\mathrm{j}\Omega)$ can be derived as:

$$C_p(\mathrm{j}\Omega) = \frac{\mathrm{Im}\{Y_p(\mathrm{j}\Omega)\}}{\Omega} \tag{13}$$

Then, this curve is fitted in correspondence of each mode through Eq. (11), determining $|k_{i,p}|$, $C_{i,p}$, $\omega_{i,\mathrm{all}}$, ζ_i and $\hat{L}_{i,p}$. Once $|k_{i,p}|$ is known for many different modes, s_p can be calculated by Eq. (3).

Before calculating s_p, a second fitting procedure can also be performed to refine the match between the measured and the reconstructed curve on a wide frequency range. Starting from the single-degree-of-freedom identifications on a series of subsequent modes (from the hth to the gth) carried out above, a global fit on all the considered modes can be performed by keeping the values found before for $C_{i,p}$ (exception made for $C_{g,p}$), $\omega_{i,\mathrm{all}}$, ζ_i for all the modes, and looking for the best possible match by changing $k_{i,p}$, $C_{g,p}$ and $\hat{L}_{h,p}$. According to

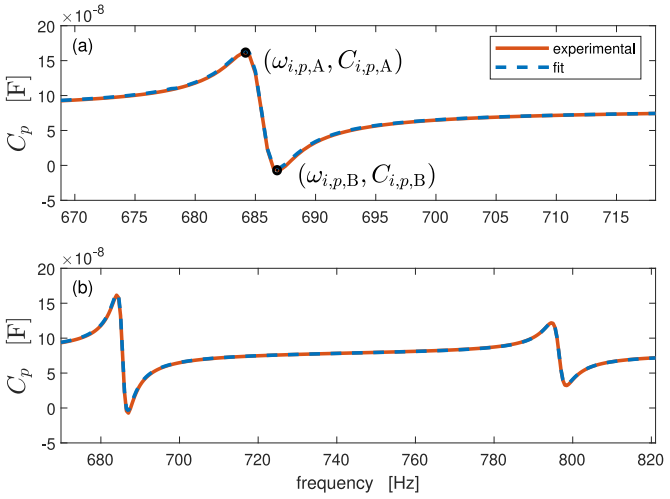

Fig. 2. Single- (a) and multi- (b) degree-of-freedom fit for an experimental curve measured during experiments (see Section 5). Extreme values of the curve in plot (a) are indicated through the coordinates $(\omega_{i,p,\mathrm{A}}, C_{i,p,\mathrm{A}})$ and $(\omega_{i,p,\mathrm{B}}, C_{i,p,\mathrm{B}})$.

the above mathematical treatment, the capacitance curve valid between ω_h and ω_g and used for this additional fit is:

$$C_p(\mathrm{j}\Omega) = C_{g,p} - \frac{1}{\Omega^2 \hat{L}_{h,p}} + \mathrm{Re}\{\sum_{i=h}^{g} \frac{k_{i,p}^2 \omega_{i,\mathrm{all}}^2 C_{i,p}}{-\Omega^2 + 2\mathrm{j}\zeta_i \omega_{i,\mathrm{all}} \Omega + \omega_{i,\mathrm{all}}^2}\} \tag{14}$$

Fig. 2 shows an example of result of a single-degree-of-freedom fit in plot (a) and of the additional multi-degree-of-freedom fit in plot (b). The measured curve comes from the set-up described in Section 5 for the experimental activity.

In this work, the two subsequent fitting procedures will be always applied one after the other, and the method will be referred to as method 1.

3.2. Second method

This method requires to carry out single-degree-of-freedom fit on only two modes of the system and is proposed as an approach for simplifying the procedure of Section 3.1. Indeed, according to Eq. (12), the following relation can be written:

$$C_{h,p} = C_{h+1,p}(1 + k_{h+1,p}^2) = \cdots = C_{g,p} \Pi_{i=h+1}^{g} (1 + k_{i,p}^2) \tag{15}$$

which can be rearranged as:

$$r_{p,h,g} = \frac{C_{h,p}}{C_{g,p}} = \Pi_{i=h+1}^{g} (1 + k_{i,p}^2) \tag{16}$$

This implies that deriving the value of $r_{p,h,g}$, by finding those of $C_{h,p}$ and $C_{g,p}$ with two single-degree-of-freedom fits on the experimental curve of C_p, one has an index already dependent on the values of the $k_{i,p}$ of modes between the hth and gth. Therefore, $r_{p,h,g}$ can be directly used to calculate a damage index $\lambda_{p,h,g}$ to monitor in place of s_p:

$$\lambda_{p,h,g} = |r_{p,h,g} - r_{p,h,g,\mathrm{u}}| \tag{17}$$

where $r_{p,h,g,\mathrm{u}}$ refers to the healthy (or reference) condition. This method is referred to as method 2.

3.3. Third method

The method presented here can be seen as another simplification of the method described in Section 3.1 but different from that in Section 3.2. Indeed, an analytical rearrangement allows avoiding here any numerical fit of the measured C_p curve. The method shown here works mode by mode and requires that the term $1/(\Omega^2 \hat{L}_{i,p})$ in Eq. (11) is negligible. This condition is fulfilled when modal superimposition is limited. The trend of C_p around a mode i shows two extreme points at $\omega_{i,p,\mathrm{A}}$ and $\omega_{i,p,\mathrm{B}}$ (see Fig. 2a). According to [43], the following relations hold (these relations can be derived starting from Eq. (11)):

$$\omega_{i,p,\mathrm{A}}^2 = (1 - 2\zeta_i)\omega_{i,\mathrm{all}}^2, \quad \omega_{i,p,\mathrm{B}}^2 = (1 + 2\zeta_i)\omega_{i,\mathrm{all}}^2 \tag{18}$$

At $\omega_{i,p,\mathrm{A}}$ and $\omega_{i,p,\mathrm{B}}$, the corresponding values of C_p ($C_{i,p,\mathrm{A}}$ and $C_{i,p,\mathrm{B}}$, see Fig. 2a) are [43]:

$$C_{i,p,\mathrm{A}} = C_{p,i}\left[1 - \frac{k_{i,p}^2}{4\zeta_i(\zeta_i - 1)}\right], \quad C_{i,p,\mathrm{B}} = C_{p,i}\left[1 - \frac{k_{i,p}^2}{4\zeta_i(\zeta_i + 1)}\right] \tag{19}$$

It turns out that:

$$\Delta_{i,p} = C_{i,p,\mathrm{A}} - C_{i,p,\mathrm{B}} = \frac{C_{i,p} k_{i,p}^2}{2\zeta_i(1 - \zeta_i^2)} \tag{20}$$

At this point, there are two possible ways to proceed. In case the value of $1/(\Omega^2 \hat{L}_{i,p})$ is actually negligible, relying on Eqs. (18) and (19), $k_{i,p}$ can be determined as [43]:

$$k_{i,p}^2 = 4\zeta_i \frac{(1 - \zeta_i^2)(C_{i,p,\mathrm{A}} - C_{i,p,\mathrm{B}})}{C_{i,p,\mathrm{A}} + C_{i,p,\mathrm{B}} - \zeta_i(C_{i,p,\mathrm{A}} - C_{i,p,\mathrm{B}})} \tag{21}$$

with

$$\zeta_i = \frac{\omega_{i,p,\mathrm{B}}^2 - \omega_{i,p,\mathrm{A}}^2}{2(\omega_{i,p,\mathrm{B}}^2 + \omega_{i,p,\mathrm{A}}^2)} \tag{22}$$

Once $|k_{i,p}|$ is known for different modes, s_p can be calculated through Eq. (3). This method is referred to as method 3. Nevertheless, there could be the case in which the term $1/(\Omega^2 \hat{L}_{i,p})$ could result non-negligible for some modes, or the modal superimposition could result excessive in correspondence of many modes. In this case, a different approach is to consider the expression of Eq. (20) not as exact, but as an approximation, and a new damage index $s_{p,\Delta}$ can be used in place of s_p:

$$s_{p,\Delta} = \sum_{i=h}^{g} \left| (\Delta_{i,p} - \Delta_{i,p,\mathrm{u}}) \right| \tag{23}$$

where $\Delta_{i,p,\mathrm{u}}$ is the value of $\Delta_{i,p}$ in the healthy (or reference) condition. It is noticed that, in Eq. (23), it is also possible to consider non-subsequent modes. Basically, the expression of Eq. (23) is the same of Eq. (3) with $\Delta_{i,p}$ employed in place of $|k_{i,p}|$, and $s_{p,\Delta}$ can be calculated by deriving the values of $C_{i,p,\mathrm{A}}$ and $C_{i,p,\mathrm{B}}$ at different modes from the measured capacitance curve. This allows avoiding any fit procedure. Therefore, according to Eq. (20), the damage index $s_{p,\Delta}$ is function of two quantities sensitive to damage: $k_{i,p}$ and $C_{i,p}$. Indeed, according the Eq. (12), also $C_{i,p}$ is sensitive to damage because it depends on the MEMCF of other modes (see also [41]):

$$C_{i,p} = C_{\infty,p} \Pi_{n=i+1}^{N} (1 + k_{n,p}^2) \tag{24}$$

This method is referred to as method 3b.

It is noticed that, since method 3 works on few points in frequency, good frequency resolution is required for obtaining reliable results. The same applies to method 3b.

3.4. Theoretical comparison of the three methods

The three approaches, presented above under a theoretical point of view, are characterised by different levels of procedure complexity and are also expected to show different levels of reliability in detecting damage. Their main differences are discussed here.

Method 1 is based on a fit procedure and thus uses many measured samples of the capacitance curve in frequency. This implies that possible noise on the capacitance curve can be filtered out. Obviously, the quality of the fit must be always checked to assure correctness of estimated MEMCF values, and the fit must be performed in correspondence of all the interesting modes which can make the procedure

slow. Method 2 is an attempt to simplify the procedure behind method 1. Indeed, method 2 requires to carry out only two single-degree-of-freedom fits. This not only allows making method 2 faster than method 1, but also allows choosing the two modes to fit, without any need of facing complex situations where, e.g., modes are close in frequency. Finally, method 3 and its variant 3b are somehow in the middle between the two previous methods. Indeed, method 3 requires to calculate the MEMCF (or a related quantity) for all the considered modes, but without any need of performing fits of the experimental trend of the capacitance. On the one hand, this allows simplifying the whole procedure compared to method 1 but, on the other hand, possible noise on the measured curve cannot be filtered out because few points of the curve are used for calculating the damage index. Furthermore, as mentioned above, good frequency resolution is needed for the measured capacitance curve when using method 3 (or 3b).

Different methods have been proposed and discussed here in order to find out which is the minimum level of complexity of the procedure needed for correctly calculating a damage index. The three methods will be compared in terms of results further in the manuscript.

3.5. Differences between the present method and EMI techniques

This section is devoted to evidence the main differences between the presented SHM approach and EMI methods, also addressing that the measurement method and thus the hardware needed for the two of them are nominally the same.

EMI techniques mainly work at high frequency (i.e., hundreds of thousands of Hertz, even if some applications are reported also at low frequency) [44] and are not directly related to modal quantities [45,46]. Indeed, they focus on the capability of waves to propagate through the structure in which the piezoelectric elements are integrated and damage is most of the times discovered looking for large changes of the measured impedance curves at high frequency and far away from system resonances. Conversely, the method discussed here considers indexes based on damage features related to electro-mechanical energy conversion in correspondence of system eigenfrequencies, which implies that its usual working frequency range is up to few thousands of Hertz. The considered method can also work with different types of measurements (i.e., vibration measurements).

Furthermore, EMI approaches need a size of the piezoelectric element small enough to detect small damages and, often, are sensitive to temperature variations [47]. This is a significant problem often leading to the need of tailored calibration procedures [48]. Conversely, the physical principle at the base of the method presented here does not link the size of the damage to that of the piezoelectric transducer. This is because the possible damage indexes mainly depend on the change of the mode shapes at the transducer boundaries caused by the damage, allowing for a small damage being detected by a large transducer. Finally, the proposed approach, unlike EMI methods, shows good robustness with respect to temperature variations [27].

Considering that EMI techniques often work at frequency ranges much higher than the approach proposed here, the hardware useable for the present methods is less demanding compared to that commonly used in EMI methods. Indeed, working at lower frequency implies the possibility of using lower sampling frequencies, thus allowing for poorer time-resolution compared to EMI approaches. Furthermore, the possibility of working at much lower frequency values implies less problems related to load effects [49,50] due to cables (e.g., capacitive effects) when accurate measurements are needed, which is a problem to be accounted when working at high frequency.

A final point is related to the needed frequency resolution of the proposed approach compared to that usually needed in EMI applications. There is no obvious answer, which is case dependent. Indeed, in the proposed method, the needed frequency resolution for deriving the admittance and capacitance frequency curves changes structure by structure because it is function of the eigenfrequency value of the modes considered and of the related non-dimensional damping ratios. The smoother the peaks and valleys in the measured capacitance curve are (see, e.g., Fig. 2), the poorer the needed frequency resolution can be. It is important to describe any variation of the capacitance curve with a good detail to apply the proposed methods. This is something similar to what occurs in dynamic tests to derive the frequency response functions of a system to be employed for modal extraction. Furthermore, it is noticed that frequency resolution can be also changed according to the frequency range: as an example, one typically uses poorer frequency resolution at high frequency (where peaks and valleys of the capacitance curve are usually smooth) compared to what occurs in the low frequency range. To give numbers, the resolution is 0.5 Hz in Fig. 2, as an example.

Table 1
Nominal data used for the simulations at two different temperatures. Here, ϵ_0 is the free space permittivity and it is equal to 8.854×10^{-12} F/m.

	T = 293.15 K	T = 253.15 K
Aluminium		
Young's modulus [GPa]	71.00	72.34
Poisson's coefficient	0.3	0.3
Linear thermal expansion coefficient [m/(m K)]	2.4×10^{-5}	2.4×10^{-5}
PIC151		
Poisson's coefficient	0.34	0.34
Elastic compliance S_{11}, S_{22} [m^2/N]	1.50×10^{-11}	1.55×10^{-11}
Elastic compliance S_{33} [m^2/N]	1.90×10^{-11}	1.96×10^{-11}
Dielectric constant [F/m]	$2400\epsilon_0$	$2252\epsilon_0$
Piezoelectric strain constant d_{31} [C/N]	-2.10×10^{-10}	-2.07×10^{-10}
Piezoelectric strain constant d_{32} [C/N]	-2.10×10^{-10}	-2.07×10^{-10}
Piezoelectric strain constant d_{33} [C/N]	5.0×10^{-10}	4.9×10^{-10}
Piezoelectric strain constant d_{15} [C/N]	5.8×10^{-10}	5.0×10^{-10}
Material coupling factor $\hat{k}_{31}$	0.38	0.37

Table 2
List of modes considered and not considered for the calculation of index s_p. The modes are indicated through the corresponding value of $\omega_{i,\text{all}}$ at T = 293.15 K and without any damage.

$\omega_{i,\text{all}}/(2\pi)$ values of the modes involved in the calculation of s_p for simulations [Hz]	$\omega_{i,\text{all}}/(2\pi)$ values of the modes not involved in the calculation of s_p for simulations [Hz]
53.33, 91.03, 141.72, 203.54, 275.72, 354.99, 431.82, 601,83, 700.66, 819.31, 950.60, 1467.17, 1579.39, 1755.94, 1922.73	1090.25, 1245.39, 1407.50

4. Numerical simulations

This section presents some numerical simulations to show that the use of the s_p index calculated through method 1 (see Section 3.1) allows detecting the presence of a damage even when significant temperature changes are faced by the coupled system, and that the same index calculated for different piezoelectric transducers is able to give indications about the location of the damage. Therefore, the main purpose of this section is to evidence that the calculation of the damage feature $|k_{i,p}|$ by means of impedance measurements provides the same level of reliability evidenced in [27] when estimating $|k_{i,p}|$ with vibration measurements with the piezoelectric element in open- and short-circuit conditions (i.e., using Eq. (1)).

The simulated test case structure is a cantilever beam made from aluminium, coupled to five piezoelectric patches made from PIC151. The schematic of the beam is provided in Fig. 3. The length of the beam is 770 mm, made as the series of parts coupled to a patch (length of 70 mm) and without a patch (again length of 70 cm). The length of each patch is thus 70 mm. The thickness of the beam is 1 mm, while that of each patch is 0.5 mm. The damage was simulated as a reduction of 70% of the Young's modulus in seven sections (from d = 1 to d = 7 in Fig. 3). The length of the damaged area is 5 mm in each location.

Fig. 3. Structure used for simulations.

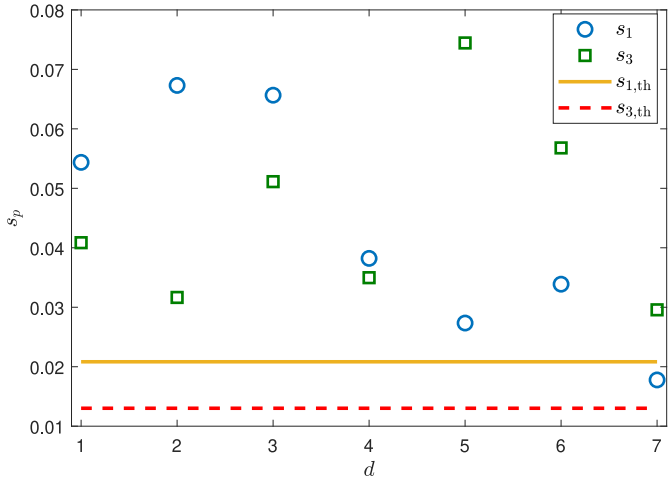

Fig. 4. s_p and $s_{p,\text{th}}$ values for patches 1 and 3 associated to different damage locations.

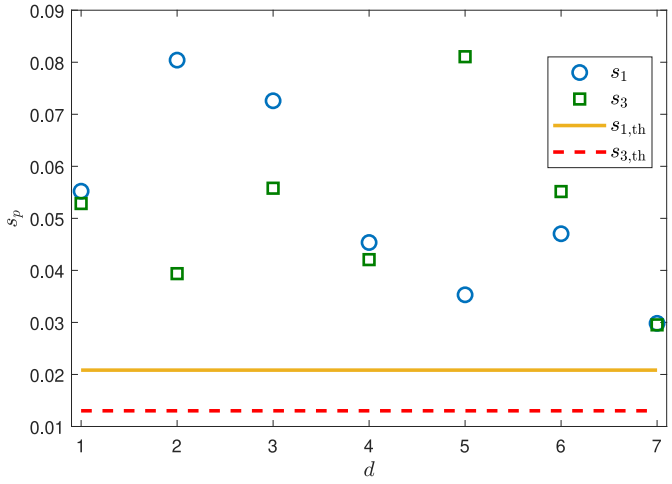

Fig. 5. s_p and $s_{p,\text{th}}$ values for patches 1 and 3 associated to different damage locations. Here, s_p values are obtained combining the $|k_{i,p,\text{u}}|$ values at T = 253.15 K with the $|k_{i,p}|$ values with damage at T = 293.15 K.

In each simulated case (i.e., beam in either healthy condition or with damage in one of the possible seven locations), finite element analysis of the system was carried out to derive the trend of C_p as function of the frequency over the first 2000 Hz (starting from 40 Hz). Then, after having obtained the C_p curves for all the patches, method 1 (see Section 3.1) was employed to derive index s_p (one for each patch).

Furthermore, the $|k_{i,p}|$ values without damage were found also for a decrease of temperature T of 40 K from the environmental temperature (i.e., from T = 293.15 K in the previous simulations, to T = 253.15 K for the present case). This allowed calculating s_p also in case of a large temperature change. These s_p values due to a thermal variation will be referred to as $s_{p,\text{th}}$ and were calculated as:

$$s_{p,\text{th}} = \sum_{i=h}^{g} \left| \left(|k_{i,p,\text{th}}| - |k_{i,p,\text{u}}| \right) \right| \tag{25}$$

where $|k_{i,p,\text{th}}|$ indicates the $|k_{i,p}|$ value at T = 253.15 K without the presence of any damage.

The data used for the simulations at the two different temperatures are reported in Table 1 and come from [27].

Here, attention will be devoted to the results related to patches 1 and 3 for the sake of conciseness. The modes considered for calculating s_p are not all those within the first 2 kHz. Indeed, those showing small $|k_{i,p}|$ values for most cases were not considered. Nevertheless, their inclusion would not change significantly the results. The list of modes considered and neglected is provided in Table 2. Fig. 4 shows the results for the mentioned patches. The s_p values (calculated at T = 293.15 K) are always larger than the corresponding $s_{p,\text{th}}$ values (exception made for patch 1 with d = 7), which in turn means that damage always produces effects on the $|k_{i,p}|$ values larger compared to that of a temperature change of 40 K. Furthermore, when the damage is closer to patch 1 than 3, s_1 results higher than s_3, and vice versa. This implies the capability of the s_p index to give indications about damage locations. When d = 4, the damage is midway between the two considered patches and, indeed, $s_1 \simeq s_3$.

Fig. 5 shows the s_p values calculated mixing the effects of temperature and presence of damage. Indeed, the two s_p values shown here are obtained considering the reference $|k_{i,p,\text{u}}|$ values with T = 253.15 K and the $|k_{i,p}|$ values with damage at T = 293.15 K. The results are still aligned with the previous conclusions, exception made for d = 7, where there is no way to obtain indications about the location of the damage since $s_1 \simeq s_3$ (however, the presence of the damage is evidenced also in this case). This is considered as a good result, also taking into account that the temperature variation is large. Furthermore, to clarify the situation related to d = 7, one could increase the number of modes involved in the calculation of s_p.

5. Experimental tests

This section presents some experimental tests in order to evidence the capability of the methods presented in Sections 3.1 to 3.3 to detect the presence of a damage, as well as to compare them.

The structure used for the tests is a cantilever beam made from aluminium, coupled to five piezoelectric patches (material PIC151) (see Fig. 6a). The schematic of the beam is provided in Fig. 6b. The length of the beam is 700 mm, made as a series of parts coupled to a patch (length of 70 mm) and without a patch (again length of 70 cm). The length of each patch is thus 70 mm. The thickness of the beam is 1 mm, while that of each patch is 0.5 mm. The damage was simulated by adding a small brick glued to the beam (see Fig. 6c) in different positions along its length (see d = 1, … ,4 in Fig. 6b). The brick was designed to have changes of $|k_{i,p}|$ quantitatively close to those due to decreases of the Young's modulus in a section between about 30% and 70% (see Section 4). As done in the simulations of Section 4, here attention will be focused on patches 1 and 3 for the sake of conciseness.

The use of a simple structure allowed focusing on the development and comparison of the proposed approaches, without any unnecessary set-up complication. Indeed, the use of MEMCF for detecting damages in more complicated structure (i.e., a truss) was already treated in [27] and additional tests are successfully running with a larger truss.

The next subsections present the results obtained with methods 1, 2 and 3b and, then, the last subsection compares the methods. Nevertheless, before these subsections, it is interesting to discuss the results of a preliminary test type. Here, four tests are considered for patch 3. Three of them are repetitions at different temperatures T (approximately 290, 293 and 296 K) of the same test type without the brick (absence of the brick is indicated with d = 0) and one with unknown temperature (however, between 290 and 296 K) and the brick

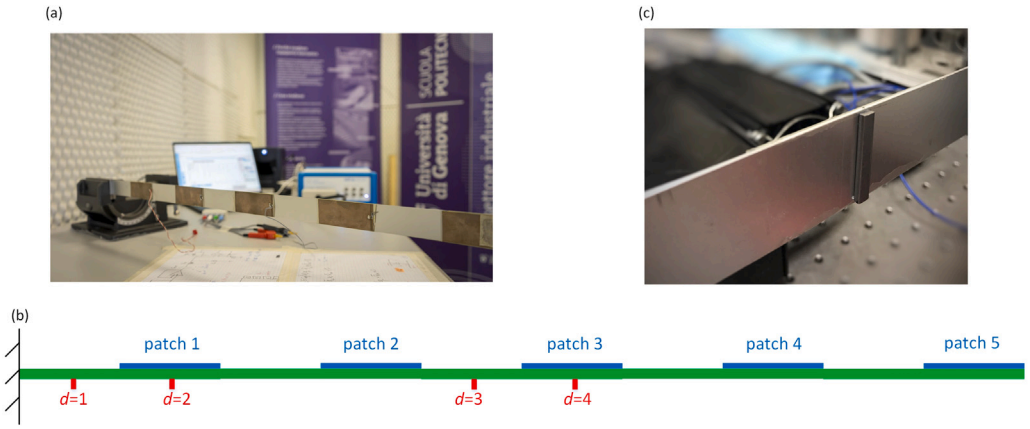

Fig. 6. A picture of the experimental set-up (a), its schematic (b), and a picture of the brick used to simulate the damage (c).

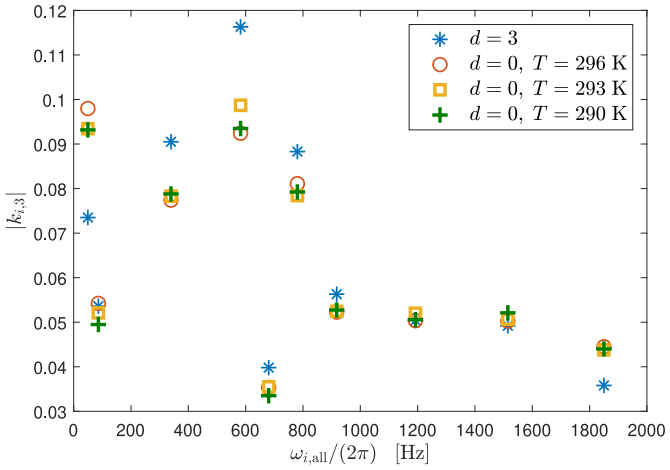

Fig. 7. Experimentally estimated $|k_{i,3}|$ values in different cases for some modes (indicated by the corresponding value of $\omega_{i,\mathrm{all}}$ for the case of $d = 3$) chosen as examples.

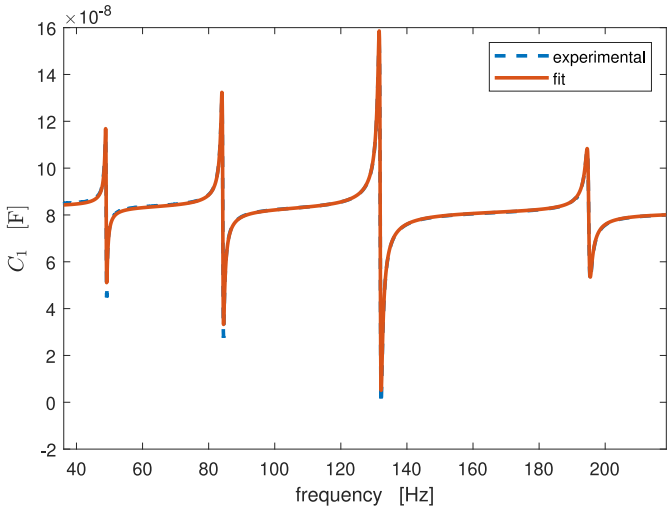

Fig. 8. Measured and reconstructed frequency trend of C_1 in case of $d = 2$.

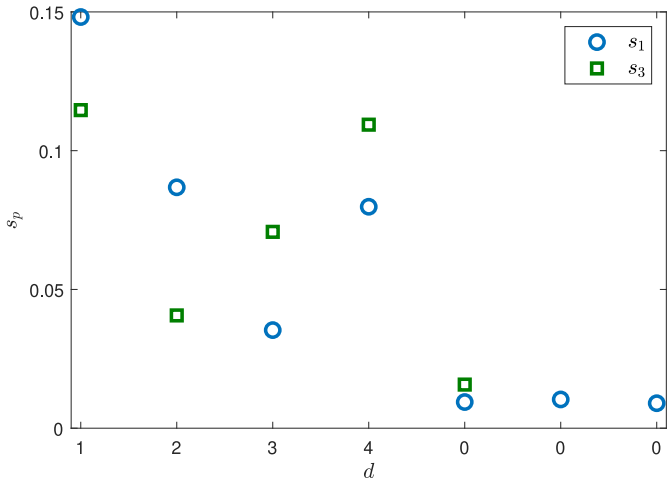

Fig. 9. Results for method 1. Zeros on the horizontal axis indicate tests without the addition of the brick.

in $d = 3$ (chosen as an example and because this position is not that causing the largest changes of $|k_{i,3}|$ values among all the considered locations of the brick). Fig. 7 shows that the change of $|k_{i,3}|$ is larger for the presence of the alteration compared to the variation of temperature for most of the modes (chosen as examples), as already evidenced in [27]. The only cases where this does not apply are modes for which the damage does not cause significant change of the considered $|k_{i,p}|$ value (e.g., modes at about 140 and 1200 Hz). For these cases, also the effect of temperature is negligible and does not cause any evident change of any $|k_{i,p}|$ value. This further confirms the robustness of the proposed damage feature to environmental variations.

Even if robustness of MEMCF to thermal shift has been experimentally validated here and in [27] for larger temperature variations (i.e., around 13 K), and also simulations confirm this robustness for temperature variations up to 40 K [27], further tests on different structures with larger thermal changes are foreseen in future to derive the limit of this property.

5.1. Method 1

Method 1 was used to calculate s_1 and s_3. Seven modes were employed, which were those always well identified in the interval 40–1000 Hz (see Fig. 8 for an example of the results of the fit on the modes between 40 and 200 Hz). Fig. 9 shows that $s_1 > s_3$ when the brick is placed close to patch 1, and vice versa (see also Fig. 6b). Furthermore, some tests without the brick were repeated in different times during a day (temperature was left uncontrolled in the lab). In all the cases, small values of both s_1 and s_3 were obtained, implying that the presence of the brick can be always detected.

Table 3
Values of s_p and β_p for method 1.

Test	s_1	β_1	s_3	β_3
$d = 0$ (ref)	$9.4{\cdot}10^{-3}$	–	$15.7{\cdot}10^{-3}$	–
$d = 0$	$9.0{\cdot}10^{-3}$	−4.3	–	–
$d = 0$	$10.4{\cdot}10^{-3}$	10.6	–	–
$d = 1$	$148.2{\cdot}10^{-3}$	1476.6	$114.6{\cdot}10^{-3}$	629.9
$d = 2$	$86.8{\cdot}10^{-3}$	823.4	$40.6{\cdot}10^{-3}$	158.6
$d = 3$	$35.4{\cdot}10^{-3}$	276.6	$70.8{\cdot}10^{-3}$	351.0
$d = 4$	$79.8{\cdot}10^{-3}$	748.9	$109.4{\cdot}10^{-3}$	596.8

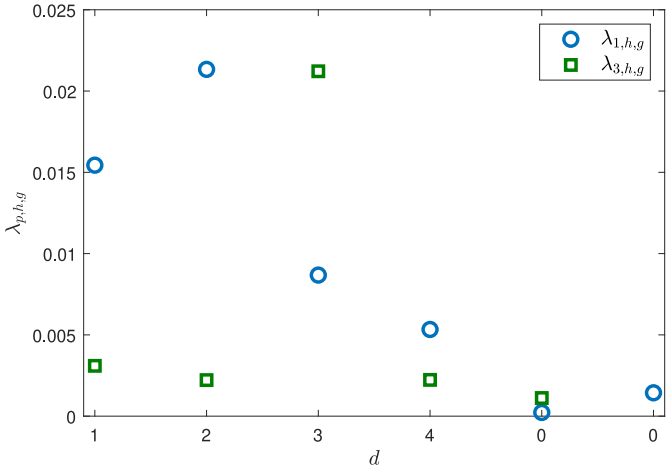

Fig. 10. Results for method 2. Zeros on the horizontal axis indicate tests without the addition of the brick.

Similar results can be found with method 3, since it uses the same features and indexes as method 1.

The results presented in Fig. 9 have been reported also in Table 3 in order to evidence also the percentage shifts of the damage index compared to a reference case for the different tests. The reference case has been chosen as the first test with $d = 0$ in Fig. 9. The percentage shift β_p in Table 3 is defined as:

$$\beta_p = \frac{s_p - s_{p,\text{ref}}}{s_{p,\text{ref}}} 100 \tag{26}$$

where $s_{p,\text{ref}}$ is the reference s_p value (as mentioned, chosen as that related to the first test with $d = 0$ in Fig. 9 and Table 3).

5.2. Method 2

With this method, the index $\lambda_{p,h,g}$ is monitored (see Eq. (17)). Mode h is chosen as a mode with $\omega_{i,\text{all}}$ at about 25 Hz, while mode g has $\omega_{i,\text{all}}$ at approximately 597 Hz. Both the mentioned eigenfrequency values are intended without the brick on the beam. Seven modes with significant $|k_{i,p}|$ values exist between the two chosen modes.

Results obtained with method 2 are presented in Fig. 10. It is evident that using results related to patch 1 allows evidencing the presence of damage in all four possible positions (i.e., $\lambda_{p,h,g}$ values clearly larger than in cases without brick). Conversely, with patch 3, the presence of the brick is found only for $d = 3$. Furthermore, $\lambda_{1,g,h} > \lambda_{3,g,h}$ for $d = 4$, even if the brick is closer to patch 3.

The evidenced problems make the use of index $\lambda_{p,g,h}$ less reliable compared to s_p for finding the presence of an alteration, as well as for determining its location. The reason is that any change of $|k_{i,p}|$ (i.e., either positive or negative) provides an increase of the value of the corresponding s_p value (see Eq. (3)), while this does not occur in $r_{p,h,g}$ (see Eq. (16)) (and, thus, in $\lambda_{p,h,g}$, see Eq. (17)).

Under a general point of view, it is good practice to consider a large distance between modes h and g (i.e., many modes between these two modes) but, due to the above-mentioned observation, this does not assure that $\lambda_{p,h,g}$ is able to properly locate the damage.

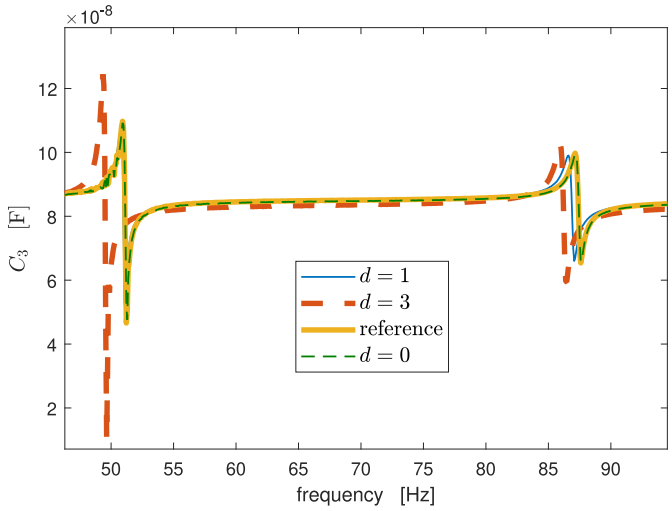

Fig. 11. Measurements of C_3 (i.e., for patch 3) as function of frequency in different cases.

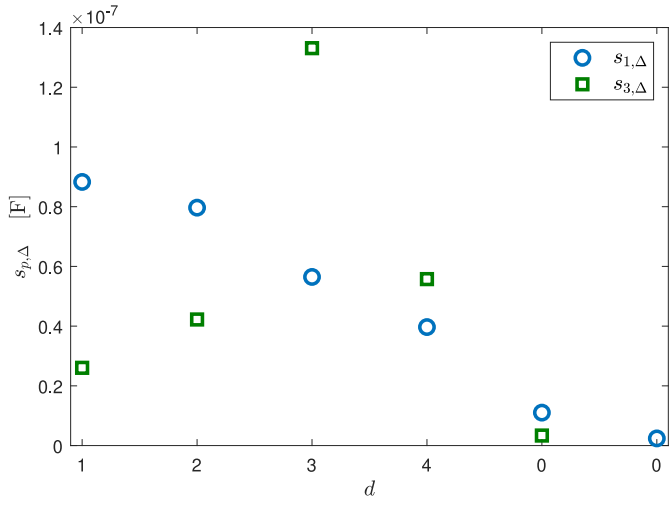

Fig. 12. Results for method 3b. Zeros on the horizontal axis indicate tests without the addition of the brick.

Table 4
Values of $s_{p,\Delta}$ and β_p for method 3b.

Test	$s_{1,\Delta}$	β_1	$s_{3,\Delta}$	β_3
$d = 0$ (ref)	$1.10 \cdot 10^{-8}$ F	–	$0.34{\cdot}10^{-8}$ F	–
$d = 0$	$0.24{\cdot}10^{-8}$ F	−78.2	–	–
$d = 1$	$8.83{\cdot}10^{-8}$ F	702.7	$2.60 \cdot 10^{-8}$ F	664.7
$d = 2$	$7.97{\cdot}10^{-8}$ F	624.5	$4.22{\cdot}10^{-8}$ F	1141.2
$d = 3$	$5.65{\cdot}10^{-8}$ F	413.6	$13.31{\cdot}10^{-8}$ F	3814.7
$d = 4$	$3.97{\cdot}10^{-8}$ F	260.9	$5.57{\cdot}10^{-8}$ F	1538.2

5.3. Method 3b

In this case, four modes (approximately between 40 and 200 Hz) were used to calculate the $s_{p,\Delta}$ values (see Eq. (23)). Fig. 11 shows a magnification on the first two considered modes for some cases chosen as examples (i.e., reference case with $d = 0$, a repetition of the same test thus with $d = 0$, a test with $d = 1$ and one with $d = 3$) in order to evidence the effect of damage on $\Delta_{i,p}$ (see Eq. (20)).

Fig. 12 shows the results in terms of $s_{p,\Delta}$ for different cases. Damage is always evidenced because there is always a significant change of the considered index compared to the case with $d = 0$ which indicates absence of the brick. Even if $s_{p,\Delta}$ (see Eq. (23)) is affected by the values of both $C_{i,p}$ and $|k_{i,p}|$ (see Eq. (20)), which could result having opposite effects sometimes (e.g., an increase of $|k_{i,p}|$ and a decrease of $C_{i,p}$ could occur together, or vice versa), the location of the brick is still correctly estimated, mainly thanks to the structure of $s_{p,\Delta}$, where both positive and negative changes of $\Delta_{i,p}$ result in a positive contribution in $s_{p,\Delta}$. Therefore, $s_{p,\Delta}$ is expected to have similar behaviour compared to s_p, even if slightly less accurate.

The results presented in Fig. 12 have been reported also in Table 4 in terms of β_p, where the index used in Eq. (26) is now $s_{p,\Delta}$ in place of s_p.

5.4. Comparison of the results obtained with the three methods

The use of methods 1 and 3 is the most reliable for detecting damage and estimate its location. This is mostly due to the way the damage index (i.e., s_p) is built. Indeed, any change, either positive or negative, in $|k_{i,p}|$ values implies a positive contribution to the damage index.

Method 2 is less reliable, especially for getting information on damage location. The reason is related to the damage index $\lambda_{p,h,g}$ for which positive and negative changes of $|k_{i,p}|$ maintain their sign and can compensate each other. This also makes $\lambda_{p,h,g}$ less sensitive to damage when it is not very close to the considered piezoelectric element. Finally, method 3b finds itself in the middle between methods 1 and 3 and method 2. However, experimental results shown here suggest that it is able to properly evidence the presence of a damage and also give indications related to the position.

Finally, since all the methods are connected to the values of $|k_{i,p}|$, they are expected to be robust to environmental changes.

6. Conclusion

This paper has dealt with an SHM method already presented in the literature based on the estimation of MEMCF of different modes in piezoelectric structures. The MEMCF of a given mode is able to quantify the efficiency of the energy conversion between mechanical and electrical domain, and vice versa, at the considered mode. Normally, MEMCFs are estimated by means of vibration measurements. The paper proposes alternative methods for estimating the MEMCFs, without relying on vibration tests. The new approaches presented here are all based on the measurement of the capacitance of each piezoelectric element attached to the structure, offering a significant simplification of the test procedure to derive the MEMCF values.

The investigated methods show different levels of accuracy in determining the presence of damage and also its location. The most accurate methods are those named methods 1 and 3 which use different approaches for deriving the MEMCF values then employed for calculating damage index s_p. Their reliability was demonstrated through both numerical simulations and experimental tests on a cantilever beam equipped with piezoelectric patches. These methods allow deriving the same damage index already proposed in the literature [27] and based on vibration measurements, just changing the method for estimation. Thus, they are expected to properly work also in case of more complicated structures for which the estimation of s_p through vibration measurements was already shown to be a reliable approach in SHM applications.

In addition, another method, named method 3b and based on damage feature and index different from those of the previous methods (but physically linked), has evidenced a good behaviour and the capability to provide information about damage location, offering at the same time a very simple procedure for estimating the damage index.

The methods proposed here allow simplifying and making faster the test procedure and the computation of the damage index, compared to the use of vibration measurements. Nevertheless, it is important to notice that some limitations exist compared to the approach based on vibration measurements. First of all, a main limitation of the methods discussed here is in case of structures with extreme modal superimposition (e.g., structures with axis-symmetry). Indeed, in such cases, the applicability of the proposed methods can be difficult, preventing the use of admittance/impedance measurements for deriving MEMCF values. Conversely, when vibration measurements are considered, these cases can be solved by either exciting the system along the principal directions, with possibility to decouple the identification of close modes, or using advanced modal identification algorithms. Another limitation of the methods presented here is that they cannot be used under operating conditions if external forcing exists in the same frequency range investigated for finding MEMCFs, because the analytical treatment implies no external forcing. Conversely, damage index calculation is possible under operating conditions by employing vibration measurements. Finally, it is evidenced that the discussed SHM approach cannot be used in presence of large nonlinear behaviour of the system.

CRediT authorship contribution statement

M. Berardengo: Writing – review & editing, Writing – original draft, Validation, Supervision, Resources, Project administration, Methodology, Investigation, Funding acquisition, Formal analysis, Conceptualization. **M. Mercato:** Visualization, Validation, Software, Investigation, Data curation. **S. Manzoni:** Writing – review & editing, Visualization, Validation, Supervision, Software, Methodology, Investigation, Formal analysis, Data curation, Conceptualization.

Declaration of competing interest

The authors declare that they have no known competing financial interests or personal relationships that could have appeared to influence the work reported in this paper.

Acknowledgements

This research has been supported by the project “CHIMERA? - is there a CHance that Indexes and Measurements of the energy conversion Efficiency Reveal system Alterations?” funded by the European Union – Next Generation EU, M4C2 I1.1, through Progetti di Rilevante Interesse Nazionale (PRIN), grant n. 20225PKHWJ (CUP: D53D23003060006).

Data availability

Data will be made available on request.

References

[1] G.M. Chatziathanasiou, N.A. Chrysochoidis, C.S. Rekatsinas, D.A. Saravanos, A semi-active shunted piezoelectric tuned-mass-damper for multi-modal vibration control of large flexible structures, J. Sound Vib. 537 (2022) 117222, http://dx.doi.org/10.1016/j.jsv.2022.117222.

[2] P. Gardonio, G.K. Rodrigues, Shunted piezoelectric patch adaptive vibration absorber set to maximise electric power absorption: A comparison between parallel and series RL-shunts, J. Vib. Control 31 (1–2) (2025) 37–50, http://dx.doi.org/10.1177/10775463241246873.

[3] Y. Zhong, X. Ma, J. Yuan, Z. Zhang, Electromechanical modelling and vibration control analysis of cyclic symmetric structures with a piezoelectric vibration absorber, J. Vib. Control (2024) http://dx.doi.org/10.1177/10775463241299858, in press.

[4] W. Huang, W. Tang, Z. Chen, L. Tang, C. Chen, L. Hou, Reinforcement-learning empowered adaptive piezoelectric metamaterial for variable-frequency vibration attenuation, Eng. Struct. 332 (2025) 120013, http://dx.doi.org/10.1016/j.engstruct.2025.120013.

[5] Y. Zhong, R. Yu, K. Zhou, Z. Zhang, Parameter optimisation of piezoelectric vibration absorber in composite cylindrical shells: A multi-modal approach to mitigate stochastic vibration, Thin-Walled Struct. 207 (2025) 112713, http://dx.doi.org/10.1016/j.tws.2024.112713.
[6] G. Shi, Y. Xia, Y. Ye, L. Qian, Q. Li, An efficient self-powered synchronous electric charge extraction interface circuit for piezoelectric energy harvesting systems, J. Intell. Mater. Syst. Struct. 27 (16) (2016) 2160–2178, http://dx.doi.org/10.1177/1045389X15624796.
[7] N. Wu, B. Bao, Q. Wang, Review on engineering structural designs for efficient piezoelectric energy harvesting to obtain high power output, Eng. Struct. 235 (2021) 112068, http://dx.doi.org/10.1016/j.engstruct.2021.112068.
[8] K. Uchino, Piezoelectric energy harvesting systems—Essentials to successful developments, Energy Technol. 6 (5) (2018) 829–848, http://dx.doi.org/10.1002/ente.201700785.
[9] T. Wang, J. Dupont, J. Tang, On integration of vibration suppression and energy harvesting through piezoelectric shunting with negative capacitance, IEEE/ASME Trans. Mechatronics 28 (2023) 2621–2632, http://dx.doi.org/10.1109/TMECH.2023.3249635.
[10] M. Zhou, Y. Wang, Y. Zhang, W. Gao, Hysteresis inverse compensation-based model reference adaptive control for a piezoelectric micro-positioning platform, Smart Mater. Struct. 30 (1) (2020) 015019, http://dx.doi.org/10.1088/1361-665X/abcc08.
[11] L. Xinliang, S. Zhengxun, L. Chen, T. Liguo, W. Guoliang, Application of adaptive inverse compensation feedforward—MPC feedback control to AFM piezoelectric micro-positioning platform, Smart Mater. Struct. 33 (7) (2024) 075020, http://dx.doi.org/10.1088/1361-665X/ad4fcf.
[12] B. Zhou, F. Thouverez, L. D., Vibration reduction of mistuned bladed disks by passive piezoelectric shunt damping techniques, AIAA J. 52 (2014) 1194–1206, http://dx.doi.org/10.2514/1.J052202.
[13] Y. Watine, B. Lossouarn, C. Gabillet, J.-A. Astolfi, J.-F. Deü, Mitigation of hydrofoil torsional flow induced vibrations by resonant piezoelectric shunt, Ocean Eng. 313 (2024) 119598, http://dx.doi.org/10.1016/j.oceaneng.2024.119598.
[14] C. Chen, A. Sharafi, J.-Q. Sun, A high density piezoelectric energy harvesting device from highway traffic – design analysis and laboratory validation, Appl. Energy 269 (2020) 115073, http://dx.doi.org/10.1016/j.apenergy.2020.115073.
[15] D. Al-Yafeai, T. Darabseh, A.-H.I. Mourad, A state-of-the-art review of car suspension-based piezoelectric energy harvesting systems, Energies 13 (9) (2020) 2336, http://dx.doi.org/10.3390/en13092336.
[16] C. Dumoulin, A. Deraemaeker, A study on the performance of piezoelectric composite materials for designing embedded transducers for concrete assessment, Smart Mater. Struct. 27 (3) (2018) 035008, http://dx.doi.org/10.1088/1361-665X/aaa7fe.
[17] V. Giurgiutiu, A. Zagrai, J. Bao, Damage identification in aging aircraft structures with piezoelectric wafer active sensors, J. Intell. Mater. Syst. Struct. 15 (9–10) (2004) 673–687, http://dx.doi.org/10.1177/1045389X04038051.
[18] J. Zhao, J. Tang, Amplifying damage signature in periodic structures using enhanced piezoelectric networking with negative resistance elements., J. Intell. Mater. Syst. Struct. 24 (13) (2013) 1613–1625, http://dx.doi.org/10.1177/1045389X13479184.
[19] M. Mohammadgholiha, J. Moll, K. Tschöke, C. Kruska, S.E. Gebhardt, L. De Marchi, Unidirectional frequency-steerable acoustic transducer for guided ultrasonic wave damage imaging, Mech. Syst. Signal Process. 229 (2025) 112505, http://dx.doi.org/10.1016/j.ymssp.2025.112505.
[20] R.K. Pandit, A. Khan, K. Balasubramaniam, B. Srinivasan, P. Rajagopal, Defect identification using sampling and outlier analysis in passive guided wave structural health monitoring, J. Intell. Mater. Syst. Struct. 36 (8) (2025) 543–560, http://dx.doi.org/10.1177/1045389X251325368.
[21] B. Chen, C. Luo, L. Xia, L. Xu, G. Yan, F. Qiu, G. Gou, Research on the measurement technology for pretension stress on small-sized bolts based on the piezoelectric ultrasonic resonance method, Materials 17 (23) (2024) 5802, http://dx.doi.org/10.3390/ma17235802.
[22] F. Sun, Z. Chaudhry, C. Liang, C. Rogers, Truss structure integrity identification using PZT sensor-actuator, J. Intell. Mater. Syst. Struct. 6 (1995) 134–139, http://dx.doi.org/10.1177/1045389X9500600117.
[23] F. Zahedi, H. Huang, Time – frequency analysis of electro- mechanical impedance (EMI) signature for physics-based damage detections using piezoelectric wafer active sensor (PWAS), Smart Mater. Struct. 26 (2017) 055010, http://dx.doi.org/10.1088/1361-665X/aa64c0.
[24] D.E. Budoya, L.M. Campeiro, F.G. Baptista, Sensitivity Enhancement of Piezoelectric Transducers for Impedance-Based Damage Detection via a Negative Capacitance Interface, IEEE Sensors J. 20 (23) (2019) 13892–13900, http://dx.doi.org/10.1109/jsen.2019.2956782.
[25] A.-L. Dreisbach, V. Yokaribas, G. Dietrich, D. Sahm, D. Pak, C.-P. Fritzen, A novel data-based approach for monitoring fatigue crack propagation in welded joints under varying ambient temperature using the electromechanical admittance, Struct. Health Monit. 22 (5) (2023) 3270–3285, http://dx.doi.org/10.1177/14759217221123976.
[26] M. Khayatazad, M. Loccufier, W. De Waele, Electromechanical impedance-based measurements for damage detection and characterization in medium-thick plates, Meas.: J. Int. Meas. Confed. 248 (2025) 116841, http://dx.doi.org/10.1016/j.measurement.2025.116841.
[27] M. Berardengo, M. Brambilla, A. Codina, N. Schena, S. Manzoni, Piezoelectric coupling as a feature sensitive to structural alterations, Mech. Syst. Signal Process. 224 (2025) 112012, http://dx.doi.org/10.1016/j.ymssp.2024.112012.
[28] J. Ducarne, O. Thomas, J. Deü, Placement and dimension optimization of shunted piezoelectric patches for vibration reduction, J. Sound Vib. 331 (14) (2012) 3286–3303.
[29] M. Berardengo, A. Cigada, S. Manzoni, M. Vanali, Vibration control by means of piezoelectric actuators shunted with lr impedances: Performance and robustness analysis, Shock. Vib. 2015 (2015) 704265.
[30] A.K. Pandey, M. Biswas, M.M. Samman, Damage detection from changes in curvature mode shapes, J. Sound Vib. 145 (2) (1991) 321–332.
[31] H. Sarmadi, A. Entezami, B. Saeedi Razavi, K. Yuen, Ensemble learning-based structural health monitoring by mahalanobis distance metrics, Struct. Control. Health Monit. 28 (2021) e2663, http://dx.doi.org/10.1002/stc.2663.
[32] K. Worden, G. Manson, N. Fieller, Damage detection using outlier analysis, J. Sound Vib. 229 (3) (2000) 647–667, http://dx.doi.org/10.1006/jsvi.1999.2514.
[33] H. Shi, K. Worden, E. Cross, A regime-switching cointegration approach for removing environmental and operational variations in structural health monitoring, Mech. Syst. Signal Process. 103 (2018) 381–397, http://dx.doi.org/10.1016/j.ymssp.2017.10.013.
[34] E. Figueiredo, G. Park, C. Farrar, K. Worden, J. Figueiras, Machine learning algorithms for damage detection under operational and environmental variability, Struct. Health Monit. 10 (6) (2011) 559–572, http://dx.doi.org/10.1177/1475921710388971.
[35] C. Roberts, L.D. Avendaño-Valencia, D. García Cava, Robust mitigation of EOVs using multivariate nonlinear regression within a vibration-based SHM methodology, Mech. Syst. Signal Process. 208 (2024) 111028, http://dx.doi.org/10.1016/j.ymssp.2023.111028.
[36] M. Pirrò, S. Pereira, C. Gentile, F. Magalhães, Á. Cunha, Damage detection under environmental and operational variability using the cointegration technique, Eng. Struct. 328 (2025) 119700, http://dx.doi.org/10.1016/j.engstruct.2025.119700.
[37] G. Cao, X. Wang, Interval deep neural networks with damage function for credible structural identification, Comput. Methods Appl. Mech. Engrg. 445 (2025) 118214, http://dx.doi.org/10.1016/j.cma.2025.118214.
[38] M. Berardengo, S. Manzoni, O. Thomas, C. Giraud-Audine, L. Drago, S. Marelli, M. Vanali, The reduction of operational amplifier electrical outputs to improve piezoelectric shunts with negative capacitance, J. Sound Vib. 506 (2021) 116163, http://dx.doi.org/10.1016/j.jsv.2021.116163.
[39] M. Berardengo, S. Manzoni, J. Høgsberg, M. Vanali, Vibration control with piezoelectric elements: The indirect measurement of the modal capacitance and coupling factor, Mech. Syst. Signal Process. 151 (2021) 107350, http://dx.doi.org/10.1016/j.ymssp.2020.107350, article ID: 107350.
[40] O. Thomas, J. Ducarne, J. Deü, Performance of piezoelectric shunts for vibration reduction, Smart Mater. Struct. 21 (1) (2012) 015008.
[41] M. Berardengo, O. Thomas, C. Giraud-Audine, S. Manzoni, Improved resistive shunt by means of negative capacitance: new circuit, performances and multi mode control, Smart Mater. Struct. 25 (2016) 075033, http://dx.doi.org/10.1088/0964-1726/25/7/075033.
[42] J. Høgsberg, S. Krenk, Calibration of piezoelectric RL shunts with explicit residual mode correction, J. Sound Vib. 386 (2017) 65–81.
[43] J.D. Richardt, B. Lossouarn, J. Høgsberg, J.-F. Deü, Sensorless calibration of piezoelectric shunts using capacitance measurements, Smart Mater. Struct. 34 (3) (2025) 035043, http://dx.doi.org/10.1088/1361-665X/adbac8.
[44] V. Giurgiutiu, Structural Health Monitoring of Aerospace Composites, Academic Press, 2016.
[45] G. Park, H. Sohn, C. Farrar, D. Inman, Overview of piezoelectric impedance-based health monitoring and path forward, Shock. Vib. Dig. 35 (2003) 451–463, http://dx.doi.org/10.1177/0583102403035600l.
[46] W. Na, J. Baek, A review of the piezoelectric electromechanical impedance based structural health monitoring technique for engineering structures, Sensors 18 (2018) http://dx.doi.org/10.3390/s18051307.
[47] G. Park, H. Cudney, D. Inman, An integrated health monitoring technique using structural impedance sensors, J. Intell. Mater. Syst. Struct. 11 (2000) 448–455, http://dx.doi.org/10.1106/QXMV-R3GC-VXXG-W3AQ.
[48] D. de Souza Rabelo, J. Steffen, R. Finzi Neto, H. Lacerda, Impedance-based structural health monitoring and statistical method for threshold-level determination applied to 2024-T3 aluminum panels under varying temperature, Struct. Health Monit. 16 (4) (2017) 365–381, http://dx.doi.org/10.1177/1475921716671038.
[49] Y. Weens, N. Idir, J. Franchaud, R. Bausière, High frequency model of a shielded 4-wire energy cable, in: Proceedings of the 2005 European Conference on Power Electronics and Applications, 2005, http://dx.doi.org/10.1109/epe.2005.219644.
[50] W. Su, H. Li, Z. Zhao, B. Zhang, C. Ji, D. He, X. Liu, Z. Wang, In-circuit impedance extraction of individual components in power converter using capacitive coupling fixture adapters method for electromagnetic interference estimation, IEEE Trans. Ind. Electron. 72 (7) (2025) 7616–7627, http://dx.doi.org/10.1109/TIE.2024.3515271.